Have Radial Velocity Surveys Missed Any Planets?

Shah Raj

Lund Observatory
Lund University

2021-EXA175

Degree project of 15 higher education credits
June 2021

Supervisor: Alexander Mustill

Lund Observatory
Box 43
SE-221 00 Lund
Sweden

Abstract

The project was aimed at numerically assessing exoplanetary systems to distinguish their capabilities of hosting additional planets. The shortcomings of the radial velocity method sometimes causes hindrance in the detection of terrestrial planets. Although modern spectrometers have evolved and improved drastically, the process of distinguishing signals from smaller planets is still difficult and cumbersome. Besides the technical difficulties, the geometry of the system is also of paramount importance in the detection process. For these reasons, we resort to other means to evaluate the potential for the existence of additional planets, especially in systems with large gaps between their known planets.

Computer simulations allow us to study such systems in great detail. We input parameters of a hypothetical planet (Earth-mass in our case) for a given range of orbits and eccentricities where we expect to find our planet, along with the other known bodies, in the simulation program, based on the orbital dynamics, the program returns an easy-to-read stability map of the system. We restrict ourselves to the habitable zones of the systems for the range of orbits. The simulations were run using the N-body integration software package REBOUND. The WHFast integrator combined with the chaos indicator, the mean exponential growth factor of nearby orbits (MEGNO), ran the simulations over a specified time period and returned the MEGNO values which were used to plot the so-called stability maps.

We looked at a total of 15 systems out of which two were found to be almost completely stable for the given initial conditions while four were found to be completely or close to being completely unstable. The rest of the eight systems had regions of both stability and instability that at times were due to rather interesting phenomena, co-orbital arrangements or suspected mean-motion orbital resonance for example. We looked more closely at HD 219828, HD 37605, HIP 67851 and Teegarden's Star. HD 219828 had a large gap between the two known planets, but due to the highly elliptical orbit of its known outer planet, which engulfed the orbital range of the hypothetical planet, it was found to be incapable of hosting an additional planet. HD 37605 was suspected to demonstrate mean-motion orbital resonance after the introduction of the hypothetical planet, though the studies did not confirm the hypothesis. HIP 67851 and Teegarden's Star were both suspected to

show co-orbital configurations in the presence of the hypothetical planet. The hypothetical planet in HIP 67851 was found to be a quasi satellite of its known outer planet, while Teegarden's Star c was found to be in a Trojan co-orbital arrangement with the speculative planet. The situation of Teegarden's Star b with respect to the introduced planet could not be assessed with certainty. One possibility is that it is in a horseshoe orbit with the introduced planet.

Populärvetenskaplig beskrivning

The existence of extrasolar planets has been long suspected but it was only relatively recently that scientists employed methods to actually detect them. Although these methods have helped us detect thousands of planets, there are still hundreds of thousands of anticipated planets which we are unable to detect; it is believed that, on average, every star has more than one planet orbiting it. Since they do not produce much light, like the stars and galaxies do, it is difficult to observe them directly. Computer simulations give us a chance at predicting the possible existence of additional unknown planets in previously known planetary systems.

The process begins by shortlisting interesting planetary systems. Three body (a star and two planets) systems are preferred since there are multiple planetary and stellar parameters to consider; this makes the process less complicated and easily approachable. Ideally, you would want to know the host star's mass and the planets' masses and their distances from the star. Small mass planets with large gaps between them are more likely to accommodate another planet. To make the study more interesting, I will be calculating the habitable zones of all the host stars and further reduce the list of targets based on whether the habitable zone lies in the gap between the planets and look for the possible existence of an terrestrial, Earth-mass planet (capable of supporting life) in that region. The habitable zone is the area around a star where temperatures are not too high or too low for liquid water to exist on a planet's surface.

Assuming there is an undetected planet in the habitable zone between the two known planets, a hypothetical planet is inserted there and the simulation is run to create a stability map for the system. The simulation is adept at detecting chaos in the system over a relatively shorter lifetime. The map produced demonstrates regions of stability and instability for the given range of the habitable zone. It is colour coded for the benefit of the user.

It is suspected that every star in our galaxy has at least one planet orbiting it. However, due to our technological limitations, we are unable to observe all of them yet. By studying the exoplanets and the exoplanetary systems, we can learn how they are formed, the multiplicity of planets in them, their mechanical properties etc. Computer simulations

can help us narrow down our search for interesting planets, especially if the purpose of the search is to look for potential habitable bodies. By knowing where to look, we can divert our energies and resources towards the more attractive and rewarding systems. The search for life is a motivation driving many experts of the time and field.

Contents

List of Figures

List of Tables

Chapter 1

Introduction

The purpose of this thesis is to assess the potential for the existence of Earth-mass planets in the habitable zones of exoplanetary systems that the radial velocity surveys might have missed during their search - planets outside the solar system are referred to as exoplanets; a definition of the habitable zone is the region around a star where liquid water can exist on a planet. The radial velocity method is good at detecting relatively large planets that lie on shorter orbits, i.e. in close proximity to their host star. Thus, it is not an ideal tool to detect smaller planets, especially those orbiting the star on larger orbits.

Specific three-body (a star and two planets) systems that have large gaps between the two known planets and whose habitable zones overlap with the gaps will be short-listed. After inserting a hypothetical, Earth-mass planet in the habitable zone of a system, its orbital dynamics will be studied and analyzed in order to evaluate its stability. A planetary system with just one planet is stable indefinitely but the introduction of more planets in a system can cause the system to destabilize due to the gravitational perturbations of the planets on each other. It should be noted that this is not always the case. Systems with more than one planet can exist harmoniously over relevant time scales, such as the Solar System.

The studies will be done by running computer simulations of the planetary motion of the two known planets and the hypothetical planet inserted in the habitable zone around their host star. The simulations survey the stability of the system for the range of orbits

(habitable zone) and the given range of eccentricities (0-0.5) of the inserted planet over a specified period producing the so-called stability maps. The stability maps of a few candidate systems will be analysed in detail to narrow down the ones worthy of more detailed investigations.

1.1 Detection Techniques

Exoplanets, generally, are not easy to detect because of their relatively small size and also because they do not radiate significantly on their own like stars. Most easily detected planets are gas giants on short orbits. Gas giants are planets that are mostly composed of gas, such as hydrogen and helium, with a small rocky core. These planets are usually large in size so when they pass in front of the star a significant fraction of the light from the star is blocked. Their pull on the host star is also greater which can be detected by the shift in the star's electromagnetic spectrum due to the Doppler effect. These properties make them more readily noticed and easily measured - these phenomena will be discussed in detail below.

Over the years, various detection techniques have been invented, some of which rely on indirect methods to reveal and identify planets. Unlike a direct observation of an object via a telescope, indirect methods are those that rely on signatures or indications that imply the existence of a planet based upon indirect observations. The two most popular of them are Doppler spectroscopy (also known as the radial-velocity method) and transit photometry (commonly known as the transit method). We briefly discuss the two methods below.

The radial velocity method relies on the fact that the star is not completely stationary when a planet is orbiting it. The gravitational pull of the planet on the star makes the star orbit around a common center-of-mass of the star-planet system. This causes a shift in the normal light spectrum of the star when observed from the Earth known as the Doppler effect. It is the shift in the frequency/wavelength of a wave with respect to an observer, i.e. when the star is moving away from the Earth the spectrum is shifted towards redder (longer) wavelengths and when it is moving towards the Earth the spectrum is shifted towards bluer (shorter) wavelengths. The stellar velocity amplitude K is defined

as Cumming:

$$K = \frac{28.4 \text{ m/s}}{\sqrt{1-e^2}} \left(\frac{M_P \sin i}{M_J}\right) \left(\frac{P}{1 \text{ yr}}\right)^{-1/3} \left(\frac{M_\star}{M_\odot}\right), \tag{1.1}$$

where M_P and P is the mass and the period of the planet orbiting the star respectively, M_J is the mass of Jupiter, i is the inclination of the orbital plane, $M_\star$ is the stellar mass and $M_\odot$ is the solar mass. Fig. 1.1 (taken from: The European Space Agency (2019)) below illustrates the mechanism. This method provides us with the semi-major axis and the minimum mass of the planet, assuming the planet is on a circular orbit.

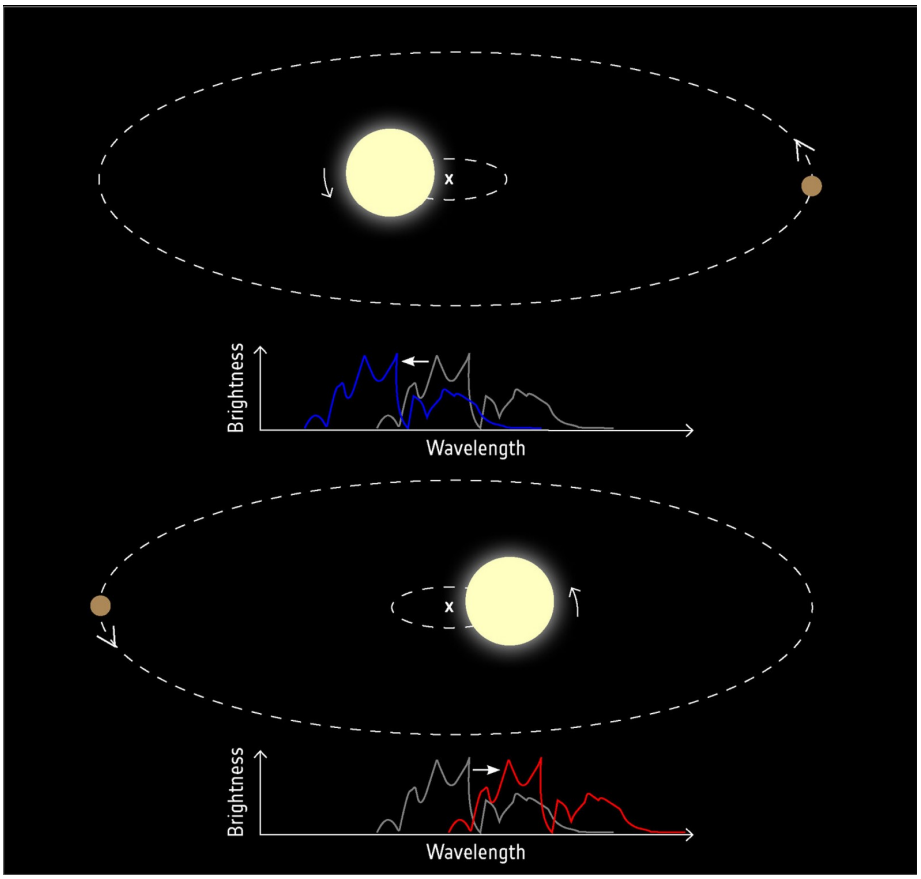

Figure 1.1: Illustration of the radial velocity method. The star and the planet orbit a common center of mass. Notice how the stellar spectrum shifts towards shorter wavelengths as the star moves towards the observer while shifts towards longer wavelengths on the journey away. Image taken from: The European Space Agency (2019); `https://www.esa.int/ESA_Multimedia/Images/2019/02/Detecting_exoplanets_with_radial_velocity`

Although the radial velocity method is one of the most popular methods for finding planets, it has some limitations. If the planetary system under observation does not lie on the

same plane (edge-on) as our line-of-sight, then we would not measure the full velocity of the star, hence a smaller mass of the planet is calculated. Unless the inclination of the orbital plane of the planet with respect to our line-of-sight is known, the measured mass is believed to be less than or equal to the true mass of the planet. While there are second and third generation spectrographs in use today that are much more precise than their previous generations, there are still limitations that make it difficult to detect Earth-mass planets, especially those that are on orbits far out from the star. For example, if there are two giant planets orbiting a star and there exists a smaller planet on an orbit in the gap between them, there is a chance that the smaller planet escapes detection. Eq. 1.1 quantifies the velocity amplitude signal which, as observed, becomes increasingly weak as M_P becomes smaller.

The transit method is another indirect way of confirming the existence of a planet around a star. This is based on the passage of the planet in front of the star that results in a drop in the brightness of the star. Fig. 1.2 (taken from: NASA Ames (2012)) illustrates the mechanism of the method. Since this drop is periodic and consistent, it yields the period and the radius of the planet. Combined with the knowledge of the mass from the radial velocity method one can find the mass density of the planet that can be used to analyse the physical structure of the planet, for example whether it is a gas giant like Jupiter or a rocky ball like the Earth.

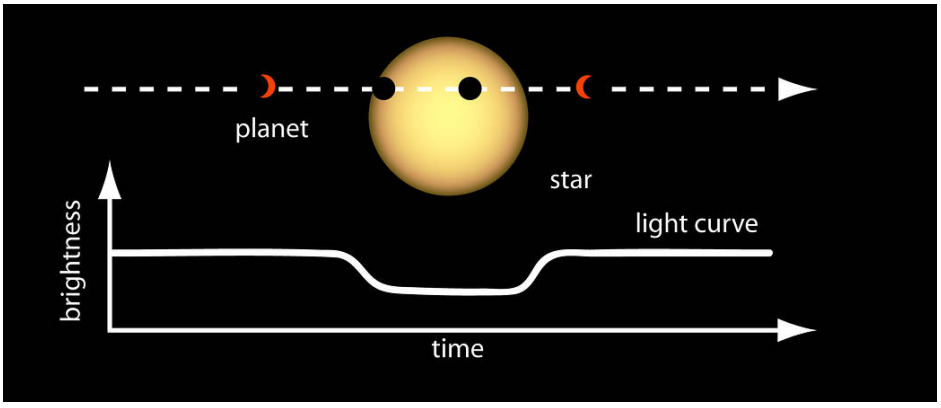

Figure 1.2: Illustration of the transit method mechanism. Notice how the stellar brightness drops as the planet passes in front of the star. Image taken from: NASA Ames (2012); `https://www.nasa.gov/mission_pages/kepler/multimedia/images/transit-light-curve.html`

However as for all methods, there are limitations to the transit method too. In order to observe the transit, the orbital plane must be edge-on to our line-of-sight. For example, if there are two planets orbiting a star with a large gap between them, it is possible that the transit survey missed a planet between those two because the planet in the gap did not align with our line-of-sight; even a slight inclination of the orbital plane with respect to our line-of-sight could completely hide a planet in that orbit. This calls for additional investigation via other means to confirm the existence of planets in any system. Besides that, this method also has other weaknesses, one of which is the likelihood of false positives in binary systems (two-star systems orbiting around their common center-of-mass). If the star is a binary and the companion is a low mass star, such as a white or a brown dwarf, then the eclipse would still pick it up as a planet. For this reason, the radial velocity method is necessary for the confirmation of a planet.

Chapter 2

Background

In this section, we will explore the mathematical relations and the physical phenomena that will help us examine the stability of the three-planet systems. Computer simulations will be run on our narrowed down systems of interest to study their mechanical dynamics after the insertion of a hypothetical planet in the system. The evolution of the planet's trajectories will be studied for the given initial conditions (see Rein and Tamayo (2016)).

2.1 Mass-Radius Relation

Mass and radius are the two fundamental properties of most heavenly bodies. The two detection techniques discussed in the previous section provide either the mass (via radial velocity method) or the radius (via the transit method) of a planet, depending on the technique used. So if a planet is detected using only one of the methods it will only be possible to measure one of the properties. Since most planets detected up to date are from transit surveys and we require the mass of planets for the sake of dynamical studies that are to be conducted in this project, we require a mass-radius relation to estimate the masses of the planets only detected via the transit method. According to Chen and Kipping (2017), for planets of radii roughly between 1 and 10 $R_\oplus$ (Earth radii), the mass-radius relationship is:

$$R \approx M^{0.59}, \tag{2.1}$$

where R is the radius and M is the mass of the planet expressed in Earth radii and masses.

2.2 Orbital Elements and Resonance

Orbits can be distinctively defined by parameters called orbital elements. There are six conventional elements, collectively known as the Keplerian elements. Fig. 2.1 represents the elements graphically:

- Semi-major axis (a) - average of the sum of the pericenter (closest point from the central body on an elliptical orbit) and apocenter (furthest point from the central body on an elliptical orbit).
- Eccentricity (e) - amount of deviation of a conic section from being circular.
- Inclination (i) - angle between the orbital plane and the plane of reference.
- Longitude of ascending node (Ω) - angle measured from the vernal point (Υ) in the reference plane to the ascending node that gives a horizontal definition to the ascending node (point where the orbit passes upward through the reference plane).
- Argument of periapsis (ω) - angle between the ascending node and the periapsis. It describes the orientation of the ellipse in the orbital plane.
- True anomaly (ν) - position of the orbiting body on the orbit at a certain time. It is marked from the line connecting the center of mass and the periapsis.
- Mean anomaly (M) - just like the true anomaly, mean anomaly tracks the angular position of the object on an orbit but unlike the true anomaly, this angle keeps increasing linearly with time. This is not one of the six conventional elements but it is sometimes used instead of the true anomaly.

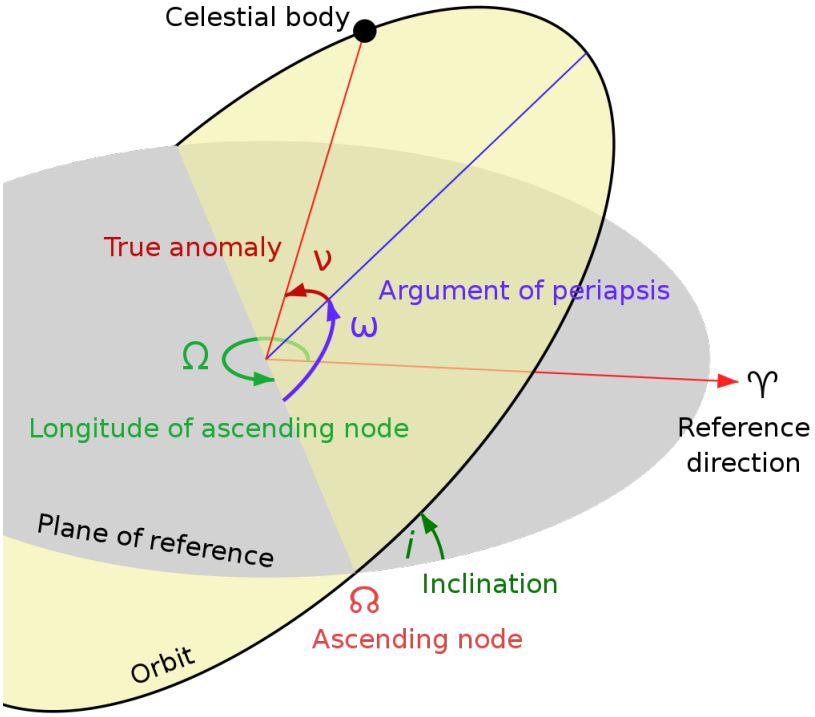

Figure 2.1: The yellow plane describes the orbital plane while the grey plane describes the reference plane. Their intersection is known as the line of nodes. It connects the center of mass with the ascending and descending nodes. Image taken from: Wikipedia (2021) (`https://en.wikipedia.org/wiki/Orbital_elements`).

The orbit of a planet around a star is invariant if it is the only body in orbit around the star. However, if there is more than one planet in a system, the planets pull on each other such that their orbits undergo changes. These changes are the greatest when the ratio of the planets' periods is an integer. This phenomenon is known as the mean-motion orbital resonance. It can either work to stabilize or destabilize a system in the long run, depending on the system's geometry. In most cases, two bodies closely approaching each other tend to destabilize the system. However, if the bodies never approach each other closely enough, then the resonance could work in the system's favour to stabilize it, for example, the 2:3 resonance of Neptune and Pluto in our Solar System. More specifically, if one of the bodies transfers a net angular momentum to the other body on their closest meeting, then the orbits would change over time in a self-correcting manner.

2.3 Hill Sphere

Celestial bodies define a sphere of influence around themselves where the gravitational pull of a body dominates. An object is gravitationally bound to a body when it falls within that sphere of influence, for example, the Moon orbiting the Earth. The sphere of influence is also commonly known as the Hill sphere, which is defined for a planet by the mass of the star as well as the mass, semi-major axis, and eccentricity of the planet. The single body hill sphere r_H is defined as (Murray and Dermott, 2000),

$$r_H \approx a(1-e)\left(\frac{m}{3M_\star}\right)^{1/3}, \tag{2.2}$$

where a is the semi-major axis and m is the mass of the planet, and $M_\star$ is the mass of the central star. A more general form of it is called the mutual Hill sphere R_H - defined for two planets and the star in a system. The origin of the sphere in this context can be taken to be the center of mass of the two bodies. The following equation states the mutual Hill sphere relation as stated in Pu and Wu (2015):

$$R_H = \frac{a_1 + a_2}{2}\left(\frac{m_1 + m_2}{3M_\star}\right)^{1/3}. \tag{2.3}$$

As a general rule, greater spacing between planets in a system means greater stability. According to Pu and Wu (2015), a simple method to quantify this notion is by defining planet spacing as a unitless number K:

$$K = \frac{a_2 - a_1}{R_H}. \tag{2.4}$$

For numerical simulations run over a billion years, the probability for a system to remain stable begins to approach 1 for $K > 10$ (Pu and Wu, 2015).

2.4 Orbital Stability and Chaos

As of today, planets are believed to be formed in a disc of gas around the star known as the protoplanetary disc. Some of the dust and gas condenses into protoplanets and then into planets. The remaining dust and gas is eventually cleared by the stellar radiation pressure, clearing the planets' orbits.

After the formation of planets, the long-term stability of a system depends on a number of factors, such as the packing of the planets, orbital parameters as well as the mean-motion orbital resonance (see Petit et al.). For systems with more than two planets, there is no exact solution to the equations of motion. The level of complexity increases with the increasing number of bodies in a system, which makes it increasingly hard to analytically understand the origin of dynamical instability (Pu and Wu, 2015). This calls for the need to study orbital mechanics computationally. Computer simulations help us survey systems by running simulations over them for varying initial conditions.

Chaos plays an important role in the evolution of a planetary system. Although there is no universally accepted definition of chaos, in the context of this paper, we will use it as is defined in Murray and Dermott (2000): if the final dynamical state of an object is sensitively dependent on its initial conditions then it is said to exhibit chaotic motion. For example, the exponential divergence of two planetary orbits, or their intersection based on the planets' initial conditions.

2.5 REBOUND with the MEGNO Indicator

REBOUND (Rein and Liu) is an N-body integrator software package that can be installed and operated in Python. We use the WHFast integrator under REBOUND. The WHFast integrator is a symplectic integrator that conserves energy and angular momentum better than the non-symplectic class of integrators. Stellar and planetary parameters of the known planets and the star, as well as the initial conditions of the hypothetical, inserted planet are fed to the code. The code then runs simulations by analysing and computing pair-wise interactions between all the bodies in the system over a specified integration time period for a given time-step.

Although REBOUND is capable of running direct N-body integrations by using an appropriate integrator, we will also use the mean exponential growth factor of nearby orbits (MEGNO) (Rein and Tamayo, 2016) algorithm under REBOUND in combination with the WHFast integrator (Rein and Tamayo, 2015) for our case. MEGNO is a chaos indicator capable of detecting chaos in a system over a rather shorter computational time period as

compared to a direct N-body integration that would not employ MEGNO or any other chaos indicator in order to evaluate a system's stability. It is defined by,

$$Y(\gamma(t)) = \frac{2}{t}\int_0^t \frac{\dot{\delta}(\gamma(t'))}{\delta(\gamma(t'))}t'dt', \tag{2.5}$$

where $\delta(\gamma(t))$ is an arc of an orbit, $\dot{\delta}(\gamma(t))$ is its time derivative - the rate at which the arc distance is covered, and t is the total integration time elapsed up to the end of each timestep (see Cincotta et al. (2003)).

For chaotic orbits, the algorithm provides linearly increasing numerical values with time for a given set of initial conditions; values ranging from about 2 to infinity. Values about 2 are considered the most stable and those greater than 3 are, generally, considered unstable (Cincotta et al., 2003). For the ease of use and making the plots easy to read, the numerical MEGNO values are translated into a colour scheme, such that the regions of stability/instability are easily identifiable on a plot.

2.6 Habitable Zone

The habitable zone (HZ) is the range of orbits around a star where liquid water can be sustained on a planetary body in that region. Distances of the HZs from stars will vary depending on the type of star. As a general rule, cooler stars will have their HZs closer to them, while hotter stars will have their HZs much farther out.

The HZs not only depend on the stellar flux but also on the planet receiving the flux. Several planetary parameters dictate the HZ boundaries, such as the mass of the planet, the kind and the quantity of gases composing the planet's atmosphere etc. However, the mass of the planet should be sufficient in order to be able to sustain an adequate atmosphere which helps in maintaining the long-term presence of liquid water on the surface. Primarily, it is the job of the greenhouse gases to support a fairly constant temperature and pressure to sustain liquid water, but an increase or decrease in the amount of such gases will result in either evaporation or freezing of the water, respectively.

Besides the absorption of the stellar energy, a planet might also reflect some of the ra-

diation received from the star due to its surface properties. This is known as the albedo - fraction of the incoming stellar flux reflected back into the space.

We will follow Kopparapu et al. (b) to calculate the HZ boundaries. The effective stellar flux (S_{eff}) incident on a planet for stars with effective temperatures (T_{eff}) in the range 2600-7200 K is:

$$S_{\text{eff}} = S_{\text{eff}_\odot} + aT_\star + bT_\star^2 + cT_\star^3 + dT_\star^4, \tag{2.6}$$

where $S_{\text{eff}_\odot}$ is the solar flux, $T_\star = T_{\text{eff}} - 5780$ K, and a, b, c, d are pre-defined coefficients. S_{eff} can be translated into units of distance by:

$$d = \left(\frac{L/L_\odot}{S_{\text{eff}}}\right)^{0.5} \text{AU}, \tag{2.7}$$

where $L/L_\odot$ is the fraction of the stellar luminosity relative to the solar luminosity. d in Eq. 2.6 is a parameter while in Eq. 2.7 it defines distance. Stellar luminosity relative to solar luminosity can be calculated using the Stefan-Boltzmann equation:

$$L = \left(\frac{R_\star}{R_\odot}\right)^2 \left(\frac{T_\star}{T_\odot}\right)^4 \text{L}_\odot, \tag{2.8}$$

where $R_\star$ is the stellar radius.

Chapter 3

Method

The goal here is to shortlist relevant systems downloaded from the NAS (2021), calculate their HZs, place the Earth-mass planet in the HZs of the systems and simulate the orbital dynamics to check whether the system is stable or demonstrates chaos.

3.1 Shortlisting Interesting Systems

We start by downloading the data of two-planet systems from the NAS (2021) (`https://exoplanetarchive.ipac.caltech.edu`) as a csv file. The file was read in Python environment using the pandas library. All the sorting and reduction of data was done using DataFrame. Since only the systems whose semi-major axes were provided in the archive were relevant, all the other systems missing semi-major axes values were eliminated. I also dropped all those systems whose stellar mass, effective temperature or stellar radius were not provided. I further reduced the list of targets by removing systems whose planets' masses were not given in the archive and their radii were greater than or equal to 10 $R_\oplus$. This was done because over approximately 10 $R_\oplus$ the mass-radius relation (Eq. 2.1) no longer holds. The radius remains fairly constant for a range of masses above 200 $M_\oplus$ (see Chen and Kipping (2017)). For the remaining systems, missing planetary masses were estimated using Eq. 2.1. I also removed the systems whose time of conjunction or epoch of periastron were not provided because these orbital parameters were going to be needed as initial conditions to integrate the systems. We will be studying coplanar systems therefore we do not consider inclination.

Planetary and stellar masses were converted from Earth mass and solar mass units to kilograms, and the mutual Hill radii of the systems and their corresponding K-values were calculated using Eqs. 2.3 and 2.4 respectively. I removed all those entries whose K-values were less than 10 as the probability of a system that it will remain stable begins to approach 1 for $K > 10$. Some of the stellar luminosities were provided in the planetary archive. Missing stellar luminosities in other systems were estimated by the Stefan-Boltsmann equation (Eq. 2.8). Lastly, I plotted the Hertzsprung–Russell (HR) diagram for the remaining systems (Fig. 4.1). The final list of systems was compiled in descending order of K-values.

3.2 Estimating the Habitable Zones

Next, the HZs of the reduced list of systems were estimated using part of the FORTRAN code (see Kopparapu et al. (a); Kopparapu et al. (b)). Firstly, I calculated the S_{eff} values for the inner (recent Venus and runaway greenhouse limit) and the outer (early Mars and maximum greenhouse limit) habitable zone boundaries using Eq. 2.6. Parameters a, b, c and d determine S_{eff} for each boundary; they were provided in the code.

Then I converted S_{eff} values into more useful and workable units of distance, astronomical units (AU), via Eq. 2.7. To ensure larger HZs around the stars in order to increase the range of orbits for the hypothetical planet, smaller inner (recent Venus ≈ 0.75 AU) and larger outer (early Mars ≈ 1.68 AU) HZ boundaries were chosen. They were mapped on a scatter plot against the corresponding stellar luminosities (Fig. 4.2). Semi-major axes of the known planets and the habitable zone boundaries of the host stars were plotted against their stellar hosts (Fig. 4.2).

3.3 Running Simulations using the MEGNO

The Python package REBOUND was used to run the simulations and to create the MEGNO stability maps. The code was fed the relevant stellar parameters - mass, and the initial conditions for the known planets - mass, eccentricity, period, argument of periastron, epoch of periastron. Since the parameters (a, b, c, d) used to calculate the habitable zone boundaries corresponded to a 1 Earth mass planet, the inserted planet's mass was,

consequently, 1 Earth mass for all systems. The code was also fed the stellar mass and the time-step for the integration for each system. I chose the time-step to be roughly 10 % of the orbital period of the inner planet of each system in order to be consistent. The WHFast integrator in the code along with the chaos indicator MEGNO mapped the stability of the systems for the given range of the semi-major axis (range of the HZ of the star between the two known planets) and the range of eccentricity (which was chosen to be between 0 and 0.5) of the inserted planet. We stop at 0.5 e because higher eccentricity orbits would mean smaller periastrons and consequently greater velocities at periastrons which would require smaller time-steps to account for those two factors, leading to longer simulation periods. Also, the climate is likely not very stable at higher eccentricities. Keeping in mind the limitations on time, as a compromise, the upper limit of the eccentricity was chosen to be 0.5.

Chapter 4

Results and Discussion

4.1 Shortlisting Systems

Stellar luminosities were needed to calculate the HZ boundaries in units of distance. Therefore, the HR diagram was plotted to ensure that the systems whose stellar luminosities were estimated using the Stefan-Boltzmann equation, due to their absence in the exoplanet archive, sit well on the HR diagram by following its characteristic shape. It can be seen in the left panel of Fig. 4.1 that the diagram retains the characteristic shape. The gap roughly between 3000-3500 K is due to the elimination of many systems due to multiple filters applied while processing the data.

As a sanity check, the inner and outer habitable zone boundaries were plotted against stellar luminosities (right panel of Fig. 4.1).

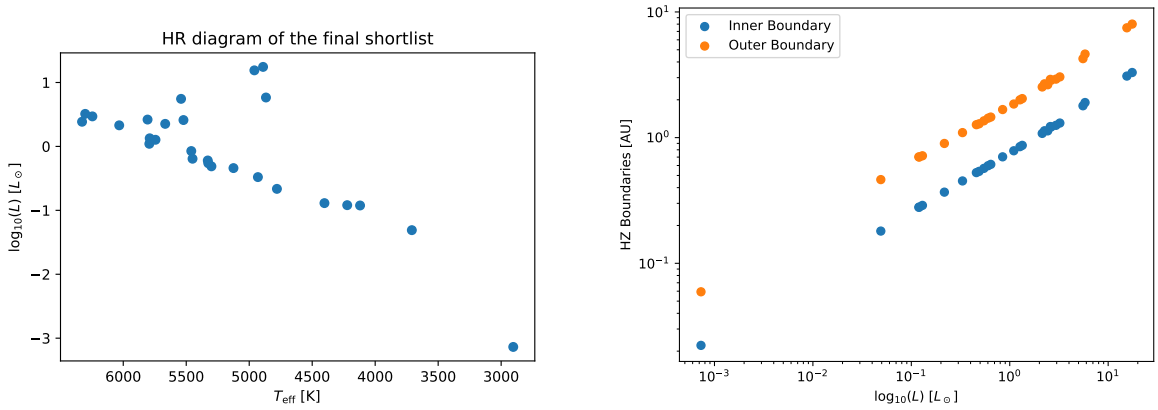

Figure 4.1: Left: HR diagram of the final shortlisted systems. Right: Inner and outer HZ boundaries against the stellar luminosities of the shortlisted systems.

Table 4.1 below summarizes the shortlisted systems and some of their properties. Fig. 4.2 represents those systems graphically by plotting the planets' semi-major axes, the systems' HZ boundaries, as well as the planets' periapsis and apoapsis on their orbits. The systems are listed in descending order of K values, with the most stable system on the top, and the least stable system on the bottom.

Table 4.1: Shortlisted systems and some of their properties. M_* is the stellar mass, $M_{\text{Pl. b}}$ and $M_{\text{Pl. c}}$ are the masses, a_b and a_c are the semi-major axss, and e_b and e_c are the eccentricities of the inner and the outer planet, respectively.

Host Name	M_* $[M_\odot]$	$M_{\text{Pl. b}}$ $[M_\oplus]$	a_b [AU]	e_b	$M_{\text{Pl. c}}$ $[M_\oplus]$	a_c [AU]	e_c	Inner HZ [AU]	Outer HZ [AU]	K-values
GJ 414 A	0.65	7.6	0.2324	0.4500	53.8	1.4000	0.1050	0.2792	0.7024	31.4
HAT-P-11	0.81	23.4	0.0525	0.2180	507.0	4.1300	0.6010	0.3683	0.8986	22.4
HD 187123	1.04	166.2	0.0426	0.0103	632.5	4.8900	0.2520	0.8680	2.0443	21.5
Teegarden's Star	0.09	1.1	0.0252	0.0000	1.1	0.0443	0.0000	0.0222	0.0593	19.0
HD 163607	1.12	249.0	0.3620	0.7441	699.5	2.3900	0.0800	1.2251	2.9077	15.6
HIP 67851	1.63	438.6	0.4600	0.0500	1900.6	3.8200	0.1700	3.2971	8.0072	13.9
HD 37605	0.94	854.9	0.2770	0.6745	1013.9	3.7400	0.0300	0.5978	1.4279	13.7
Pr0211	0.94	597.5	0.0318	0.0110	2475.9	5.5000	0.7100	0.5389	1.2884	13.3
HD 75784	1.26	317.8	1.0320	0.0970	1792.6	8.4000	0.4890	1.9018	4.6232	13.2
HD 92788	1.15	1195.0	0.9700	0.3500	1166.4	10.5000	0.4600	0.8475	1.9985	13.1
HD 38529	1.41	253.3	0.1294	0.2800	4128.6	3.6400	0.3407	1.7923	4.2514	12.8
HD 219828	1.18	21.0	0.0507	0.1010	4640.3	5.7900	0.8102	1.2150	2.8603	12.4
HD 142	1.23	397.3	1.0200	0.1700	1684.4	6.8000	0.2100	1.2531	2.9212	12.4
HD 4732	1.74	753.2	1.1900	0.1300	753.2	4.6000	0.2300	3.0885	7.4796	12.4
HD 148164	1.21	391.0	0.9930	0.5870	1640.0	6.1500	0.1250	1.0805	2.5299	12.1

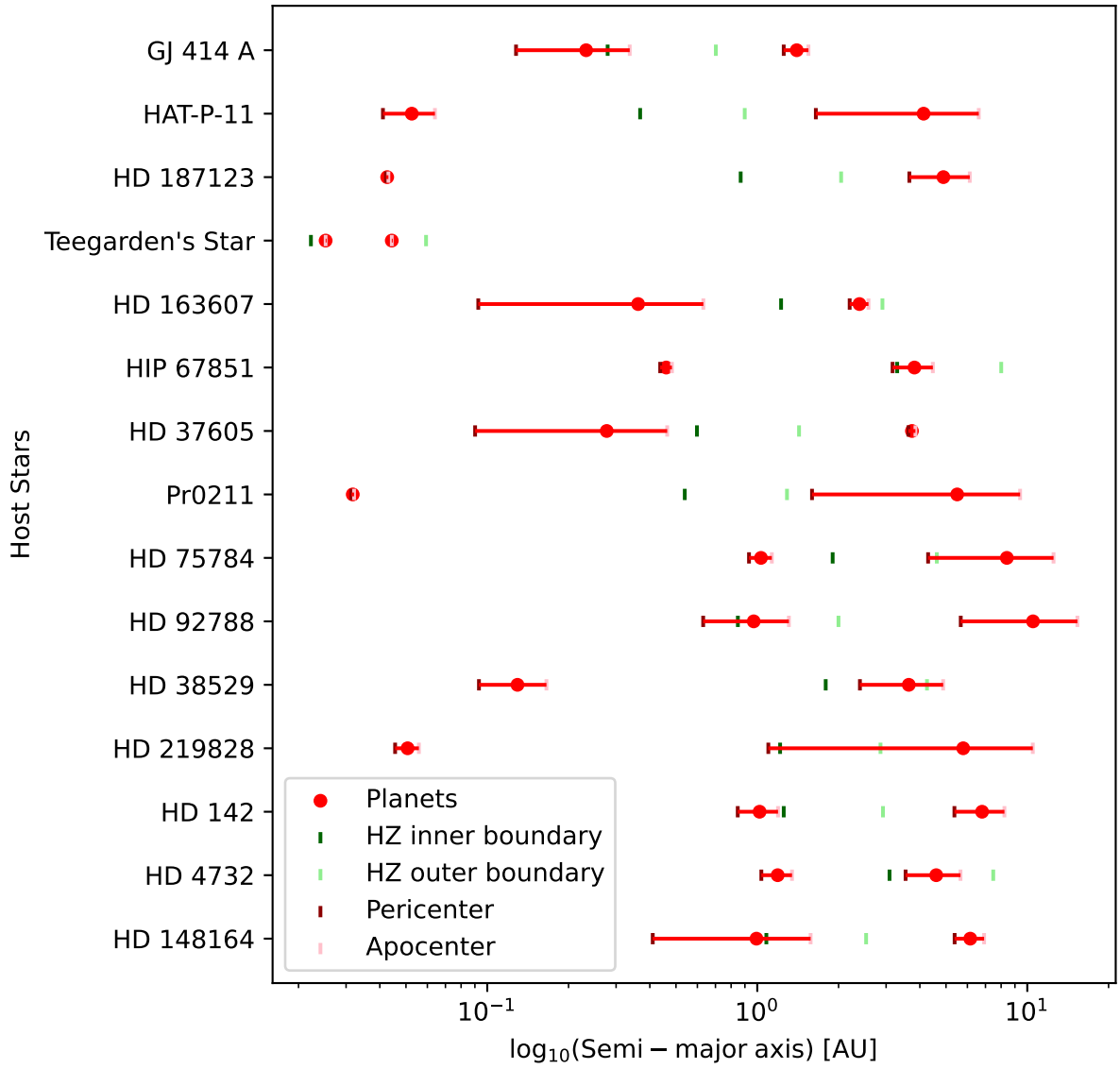

Figure 4.2: Host stars, their known planets, HZ boundaries, and their periapsis/apoapsis on their orbits plotted in descending order of K-values.

4.2 The MEGNO Maps

In this section we will analyse and discuss some of the MEGNO maps. They display the stability of the systems after the insertion of a hypothetical Earth-mass planet in the HZ in the gap between the two known planets. It should be noted that the HZ did not entirely lie in the gap in some of the systems but only partially overlapped (see Fig. 4.2).

In such cases the hypothetical planet was placed in the partial HZ between the two planets.

Table 4.2 below lists the percentage of the stable regions in the stability maps of the hypothetical systems. Two out of the 15 systems (HAT-P-11 and HD 187123) are found to be over 95% stable while four of them (HD 92788, HD 38529, HD 219828 and HD 4732) are completely or close to being completely unstable. HIP 67851 and Teegarden's star display possible co-orbital configuration which we shall explore in detail below. The white pixels mark the missing MEGNO values which I believe correspond to infinity.

HD 163607, HD 75784 and HD 142 are of particular interest as they demonstrate different levels of stability over different integration time periods. The MEGNO indicator was especially chosen as it is believed to establish the stability of a system by detecting chaos over a relatively shorter time period. However, the drastically varying results of HD 163607, HD 75784 and HD 142, integrated over 500 and 5000 years, hint at the possible shortcomings of the indicator.

I chose 4 systems (HD 219828, HD 37605, HIP 67851 and Teegarden's Star) for a more detailed analysis based on the features they demonstrated. However, this method of quantifying the amount of stable region in a system, in general, could also help us sort and choose our systems capable of hosting a terrestrial planet for more detailed investigations. MEGNO maps not discussed can be found in Appendix B.

Table 4.2: Fraction of the stable area in the MEGNO maps measured by taking the ratio of the pixels with MEGNO value less than 2.75 to the total number of pixels. HD 163607's, HD 75784's and HD 142's two values each correspond to the integration time of 500 and 5000 years respectively.

Host Name	Stable region %
GJ 414 A	46.4
HAT-P-11	98.7
HD 187123	99.6
Teegarden's Star	4.2
HD 163607	10.6, 5.2
HIP 67851	8.5
HD 37605	41.4
Pr0211	16.2
HD 75784	19.9, 5.2
HD 92788	0.9
HD 38529	0.0
HD 219828	0.0
HD 142	39.5, 18.0
HD 4732	0.3
HD 148164	9.8

4.2.1 HD 219828

Fig. 4.3 highlights the instability of the system when a third planet is inserted in the HZ in the gap between the two known planets. Although there is a large gap between the planets and the HZ lies well within the gap, upon further investigation, it is revealed that planet HD 219828 c's pericenter encloses the HZ of the system as can be seen in Fig. 4.2. Such a highly elliptical orbit means that the inserted planet's orbit would have to lie within HD 219828 c's orbit or intersect it. This would increase the chances of close encounters of the two plan-

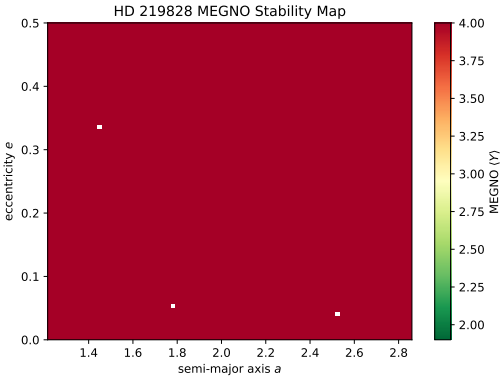

Figure 4.3: HD 219828 MEGNO stability map integrated over 500 years. Inserted planet parameters: time-step = 0.001 years, mean anomaly M = 0, $\omega = 0$.

ets, rendering the insertion unstable. It is
likely that the instability is due to the prospective close encounter of HD 219828 c and the 1 $M_{\oplus}$ inserted planet.

4.2.2 HD 37605

Along with a fairly continuous region of stability between 0.8-1.4 AU, Fig. 4.4 has green stripes throughout the map that also signify the stable regions. This was anticipated to be due to the mean-motion orbital resonance inside the system. Even though the period ratios of the innermost and the outermost planet with the inserted planet did not turn out to be exact integers (see table 4.3), some of the higher order orbital resonances of the type k:2 of the innermost planet with the inserted planet, manually marked on the stability map, lined-up with the green stripes (right panel of Fig. 4.4). Since k:1 resonances did not line-up and k:2 resonances appeared to align at higher orders, we concluded that k:2 is the strongest contender of the two resonance types for the given set of initial conditions.

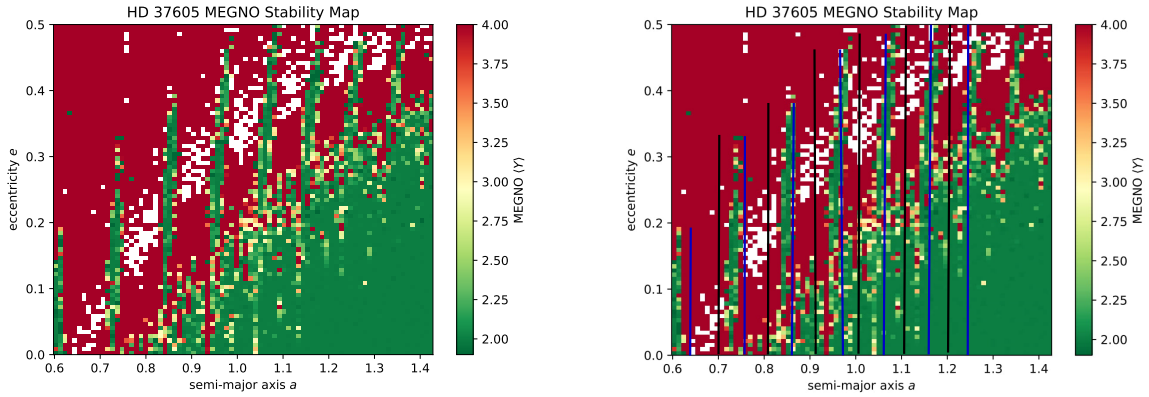

Figure 4.4: Left: HD 37605 MEGNO stability map integrated over 500 years. Inserted planet's parameters: time-step = 0.01 years, mean anomaly M = 0, ω = 0. Right: k:1 (black) and k:2 (blue) resonances marked on the map.

Table 4.3: Periods of the HD 37605 b (T_b), HD 37605 c (T_c), and the inserted planet's period (T_E) calculated at the semi-major axes of the green stripes and their ratios.

a_E [AU]	T_E [yrs]	T_b [yrs]	T_c [yrs]	$\frac{T_E}{T_b}$ [yrs]	$\frac{T_c}{T_E}$ [yrs]
0.6	0.479533	0.150720	7.452055	3.181616	15.540223
0.73	0.643540	0.150720	7.452055	4.269778	11.579767
0.84	0.794348	0.150720	7.452055	5.270355	9.381347
0.95	0.955382	0.150720	7.452055	6.338790	7.800074
1.05	1.110135	0.150720	7.452055	7.365546	6.712745
1.15	1.272443	0.150720	7.452055	8.442436	5.856489
1.25	1.441972	0.150720	7.452055	9.567226	5.167959
1.34	1.600475	0.150720	7.452055	10.618867	4.656149

4.2.3 HIP 67851

Fig. 4.5 below shows the stability map of HIP 67851. The x-axis corresponds to the tiny gap between the inner edge of the HZ and HIP 67851 c. The presence of a stable region in such a narrow gap points to the existence of a potential co-orbital configuration.

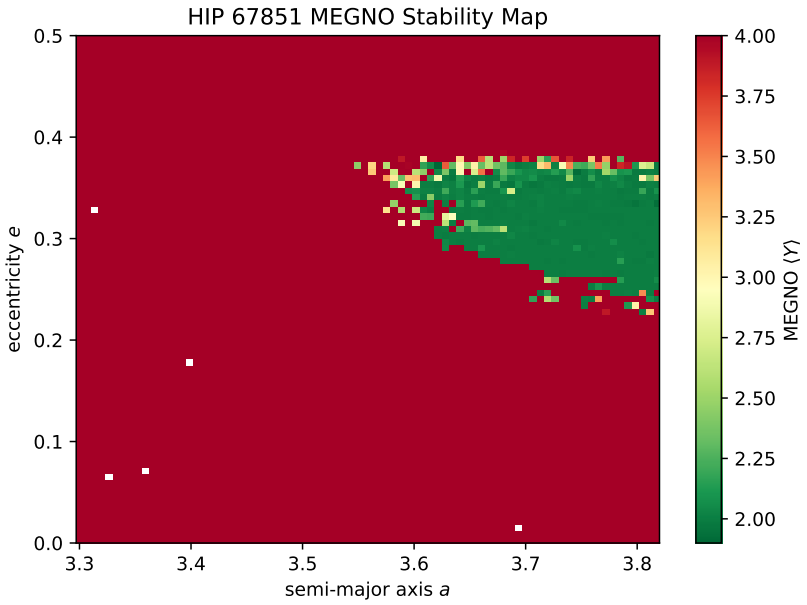

Figure 4.5: HIP 67851 MEGNO stability map integrated over 500 years. Inserted planet's parameters: time-step = 0.02 years, mean anomaly M = 0, $\omega = 0$.

Upon further inspection by taking the difference of the mean longitudes, where the mean longitude is defined as $l = \Omega + \omega + M$, of HIP 67851 c and the inserted planet at a number of locations characterized by a and e locations (see Appendix A for details), it was learnt that the inserted planet indeed librates around 0 radians in relation to the planet (Fig. 4.6). The angular Hill sphere (angle the surface of the Hill sphere makes with the line joining the center-of-mass of the star and the planet) of HIP 67581 c (roughly 1900 $M_{\oplus}$) was calculated to be 0.0872 rad, less than the amplitude of the oscillation (roughly 0.4 rad) of the inserted planet. This suggests that the inserted planet is not gravitationally bound by HIP 67581 c but rather is a quasi-satellite which orbits the central star with higher eccentricity than HIP 67581 c.

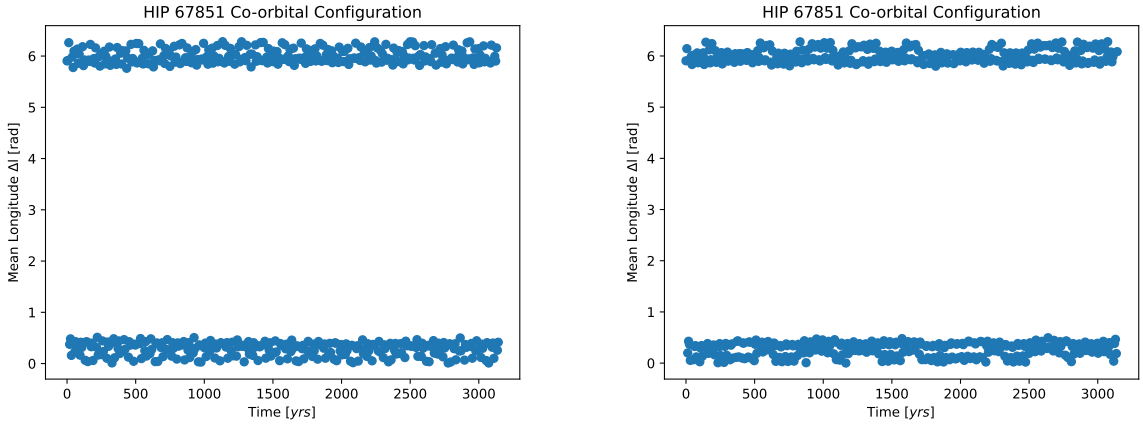

Figure 4.6: The figures display the mean longitude difference for planet HIP 67851 c and the inserted planet. There is a possible quasi-satellite arrangement with the following parameters on the left: $a = 3.7$, $e = 0.3$ and on the right: $a = 3.8$, $e = 0.35$.

4.2.4 Teegarden's Star

By the looks of the map in Fig. 4.7 below, it seems there are two regions of potential co-orbital configuration - the extreme left and right on the bottom, and a sparse region of stability in between.

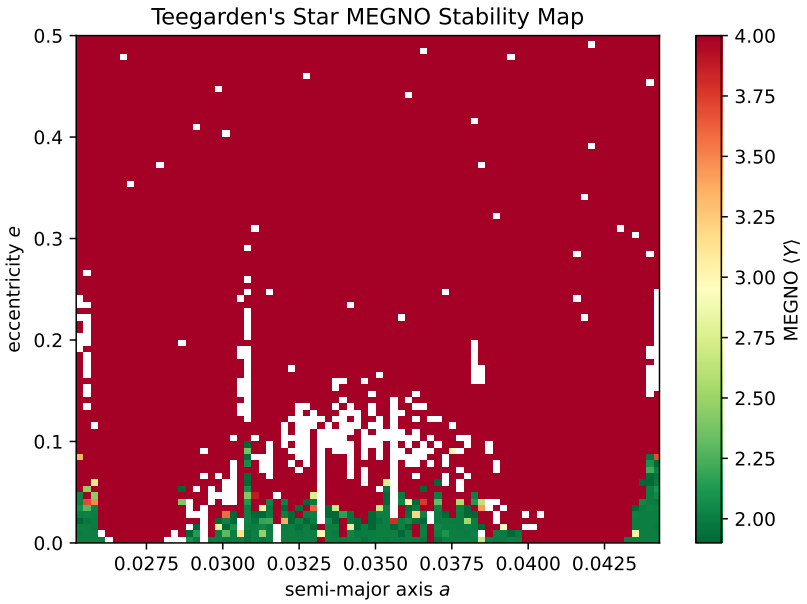

Figure 4.7: Teegarden's Star MEGNO stability map integrated over 500 years. Inserted planet's parameters: time-step = 0.001 years, M = 0, $\omega = 0$.

In Fig. 4.8 and 4.9 I plot the mean longitude difference Δl against time for the inner and outer planet, respectively. They display what was expected to be some kind of co-orbital configurations. For Teegarden's Star b (Fig. 4.8), there seems to be no apparent structure as the inserted planet seems to oscillate all over between $0 - 2\pi$ rad around it. However, planet b's angular Hill sphere (0.022 rad) is so small that it is not readily discernible from the plot whether the inserted planet's oscillation amplitude respects that boundary. This might be the case of a horseshoe orbit where the inserted planet librates about π radians from planet b.

Fig. 4.9 displays what is likely a tadpole orbit where a body oscillates at about 1.05 rad (60°) in front of or behind the other body. The oscillations are not symmetric about the mean position which is what gives it its name. From this, we deduce that the inserted planet is in a tadpole orbit with respect to planet c. It should to be noted that the mass of both of Teegarden's star b and c is approximately 1 $M_{\oplus}$ (comparable to the inserted planet).

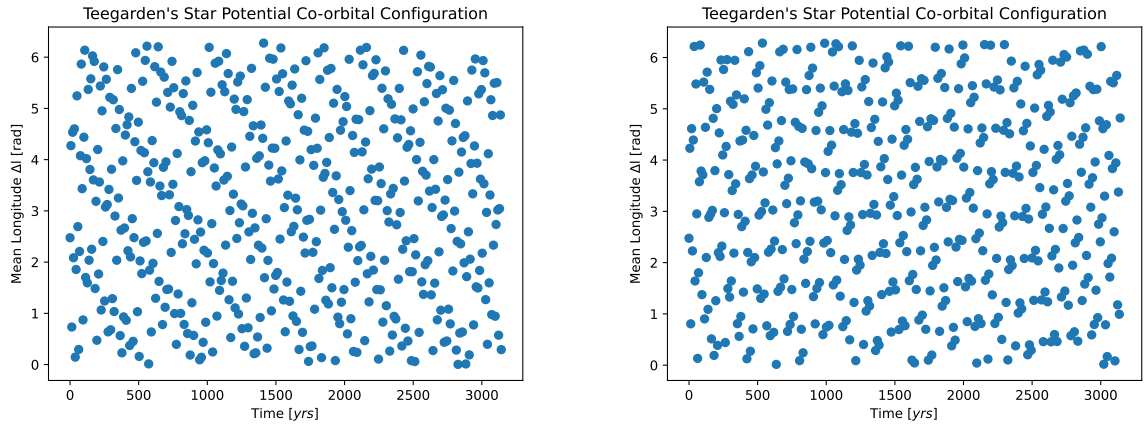

Figure 4.8: The figures display the mean longitude difference for planet Teegarden's Star b and the inserted planet with the following parameters on the left: $a = 0.025$, $e = 0.01$ and on the right: $a = 0.025$, $e = 0.02$.

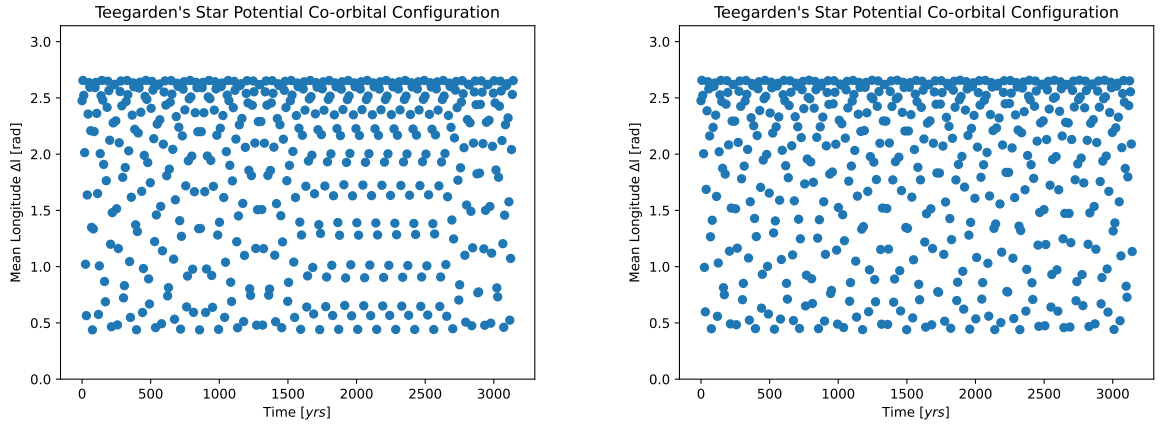

Figure 4.9: The figures display the mean longitude difference for planet Teegarden's Star c and the inserted planet with the following parameters on the left: $a = 0.0443$, $e = 0.0$ and on the right: $a = 0.0443$, $e = 0.02$.

Chapter 5

Conclusions

Simulations were run on 15 different planetary systems but due to the restriction of time only a few were discussed in the report. Planetary systems are complex structures that are most times not fully understood analytically. Usually, a computational analysis is required to integrate such systems where the wealth of orbital parameters only adds to the complexity.

We learnt that some of the systems are extremely capable of accommodating an Earth-mass planet in their HZs while others displayed a lesser tendency to do so. Some of the stability maps produced by running computer simulations were studied in greater detail. It was also learnt that by varying the initial conditions, such as the integration time, the stability of a system varied (see table 4.2). There were several other variable initial conditions - the mean anomaly, the argument of periastron, the eccentricity, that could have been explored in greater detail had time permitted.

Although systems with large gaps were anticipated to be hiding a potential planet, some of the systems that demonstrated such a feature were found to be incapable of hosting one due to the orbital dynamics of the system, such as HD 219828.

HD 37605 displayed higher order orbital resonances of the form k:2 for the given set of initial conditions.

There were some other interesting systems that displayed potential co-orbital arrangements - HIP 67851 and Teegarden's Star. The results of HIP 67851 confirmed the phenomenon and the hypothetical planet was found be to be a quasi-satellite of the outer planet in the system. The results of Teegarden's Star b, apparently, did not confirm the hypothesis unless it is in a horseshoe co-orbital configuration with the inserted planet. The results of Teegarden's Star c also confirmed the hypothesis and the inserted planet was found to be in a tadpole co-orbital arrangment with it.

HD 163607, HD 75784 and HD 142 demonstrated a distinct feature about the MEGNO indicator. They all showed a significant reduction in the stability for an increased integration time (see Table 4.2 and Appendix B for details). MEGNO was distinctly chosen as it is capable of detecting chaos over a rather short period as compared to direct N-body integrations. However, this anomaly raised concerns about the stability of the remaining MEGNO maps that could not be tested over longer periods. Had time permitted, the rest of the systems would also have been integrated for different time periods to examine whether the apparent anomaly is exclusive to the three systems for varying time periods. Integrations could also be run for longer periods to verify whether the systems eventually stabilise. MEGNO maps that could not be discussed in section 4 can be found in Appendix B.

All in all, planetary systems are an area of ongoing research and exoplanets, especially Earth-like, are being actively hunted by scouring through data provided by satellites and other, Earth-based, telescopes. Simulations such as those performed here will help us understand planetary systems better. The acquired knowledge from the simulations about the exoplanetary systems can be employed to focus our search and studies on particular systems that are more capable of hosting a terrestrial planet in their HZs, and ultimately to hosting life. I found HAT-P-11 and HD 187123 to be almost completely stable (over 95%), which could be prospective contenders in our future search for terrestrial planets.

Acknowledgements

First of all, I would like to thank my dear supervisor, Alexander James Mustill, who has acted both as a support system and a resource for me during my project. I am extremely thankful for his display of patience with me throughout the project and assisting and guiding me in times of need. I would like to thank him for making this process convenient and enjoyable for me.

I would like to express my gratitude to Sara Sultan, who has been by my side through both the thick and the thin for as long as I have known her. I cannot thank enough for the constant support and prayers of my family members: my father Ali Raj, mother Huma Gazder, sister Areeba Raj and my brother Shuraim Raj. Besides the family, I would like to thank Daniel Larsson Persson, a dear friend I made in Sweden, who has stuck by me since the start of my studies.

This research has made use of the NASA Exoplanet Archive, which is operated by the California Institute of Technology, under contract with the National Aeronautics and Space Administration under the Exoplanet Exploration Program.

Bibliography

Nasa exoplanet archive, 2021. URL `https://exoplanetarchive.ipac.caltech.edu/`. [Online; accessed 13-May-2021].

Jingjing Chen and David Kipping. Probabilistic forecasting of the masses and radii of other worlds. *The Astrophysical Journal*, 834, 2017.

P.M. Cincotta, C.M. Giordano, and C. Simó. Phase space structure of multi-dimensional systems by means of the mean exponential growth factor of nearby orbits. *Physica D: Nonlinear Phenomena*, 182:151–178, 2003. doi: 10.1016/S0167-2789(03)00103-9.

Ravi Kumar Kopparapu, Ramses Ramirez, James F. Kasting, Vincent Eymet, Tyler D. Robinson, Suvrath Mahadevan, Ryan C. Terrien, Shawn Domagal-Goldman, Victoria Meadows, and Rohit Deshpande. Habitable zones around main-sequence stars: New estimates. *The Astrophysical Journal*, 770, a.

Ravi Kumar Kopparapu, Ramses M. Ramirez, James Schottel Kotte, James F. Kasting, Shawn Domagal-Goldman, and Vincent Eymet. Habitable zones around main-sequence stars: Dependence on planetary mass. *The Astrophysical Journal Letters*, 787, b.

Carl D. Murray and Stanley F. Dermott. *Solar System Dynamics*. Cambridge University Press, 2000.

NASA Ames. Light curve of a planet transiting its star, 2012. URL `https://www.nasa.gov/mission_pages/kepler/multimedia/images/transit-light-curve.html`. [Online; accessed 1-May-2021].

Antoine C. Petit, Gabriele Pichierri, Melvyn B. Davies, and Anders Johansen. The path to instability in compact multi-planetary systems. *Astronomy Astrophysics*, 641.

Bonan Pu and Yanqin Wu. Spacing of kepler planets: Sculpting by dynamical instability. *The Astrophysical Journal*, 807, 2015. doi: 10.1088/0004-637X/807/1/44.

Hanno Rein and Shang-Fei Liu. Rebound: an open-source multi-purpose n-body code for collisional dynamics. *Astronomy Astrophysics*, 537.

Hanno Rein and Daniel Tamayo. Whfast: A fast and unbiased implementation of a symplectic wisdom-holman integrator for long term gravitational simulations. *Monthly Notices of the Royal Astronomical Society*, 452:376–388, 2015. doi: 10.1093/mnras/stv1257.

Hanno Rein and Daniel Tamayo. Second-order variational equations for n-body simulations. *Monthly Notices of the Royal Astronomical Society*, 459:2275–2285, 2016. doi: 10.1093/mnras/stw644.

The European Space Agency. Detecting exoplanets with radial velocity, 2019. URL `https://www.esa.int/ESA_Multimedia/Images/2019/02/Detecting_exoplanets_with_radial_velocity`. [Online; accessed 1-May-2021].

Wikipedia. Orbital elements, 2021. URL `https://en.wikipedia.org/wiki/Orbital_elements`. [Online; accessed 1-May-2021].

Appendix A

Code

A.1 Shortlist Interesting Systems and Estimating Habitable Zone Boundaries

```
from pylab import *
import numpy as np
from mpl_toolkits.mplot3d import axes3d
import pandas

x1 = float("nan")
# Read CSV file
df = pandas.read_csv('PS_2021.04.19_10.15.21.csv')
pandas.set_option("display.max_columns", 100) # set number of columns to
    ↪ display
pandas.set_option("display.max_rows", 1000) # set number of rows to
    ↪ display

df.dropna(subset=['pl_orbsmax','pl_orbeccen', 'pl_orblper'], inplace=True)
    ↪  # Define in which columns to look for missing values (NaN) and take
    ↪  out those rows.
df['pl_bmasse'] = df['pl_bmasse'].fillna(0) # relace 'nan' with 0s.
```

```
df['pl_rade'] = df['pl_rade'].fillna(0) # relace 'nan' with 0s.
df['st_mass'] = df['st_mass'].fillna(0) # relace 'nan' with 0s.
df['st_teff'] = df['st_teff'].fillna(0) # relace 'nan' with 0s.
df['st_rad'] = df['st_rad'].fillna(0) # relace 'nan' with 0s.
df['st_lum'] = df['st_lum'].fillna(0) # relace 'nan' with 0s.
df['pl_tranmid'] = df['pl_tranmid'].fillna(0) # relace 'nan' with 0s.
df['pl_orbper'] = df['pl_orbper'].fillna(0) # relace 'nan' with 0s.
df['pl_orbtper'] = df['pl_orbtper'].fillna(0) # relace 'nan' with 0s.
df.drop(df[(df.pl_rade >= 10) & (df.pl_bmasse == 0)].index, inplace=True)
    ↪ # Remove rows whose radii are greater than or equal to 10 and their
    ↪ planetary mass is not given
df.drop(df[df.st_mass == 0].index, inplace=True) # Remove rows with
    ↪ stellar mass = 0
#df[~df.st_teff.str.contains("a", na=False), inplace=True]
df.drop(df[df.st_teff == 0].index, inplace=True) # Remove rows with
    ↪ stellar effective temperature = 0
df.drop(df[df.st_rad == 0].index, inplace=True) # Remove rows with stellar
    ↪  radii = 0
df.drop(df[(df.pl_orbtper == 0) & (df.pl_tranmid == 0)].index, inplace=
    ↪ True) # Remove rows where both time of conjunction and epoch of
    ↪ periastron are 0
df1 =pandas.concat(g for _, g in df.groupby("hostname") if len(g) > 1) #
    ↪ Keep only duplicate entries in "Host Name"


df2 = df1.drop_duplicates(subset=['hostname'], keep='first') # keep first
    ↪ duplicate entry
PNb = df2['pl_name'].tolist()
HN1 = df2['hostname']
PRb_list = df2['pl_rade'].tolist()
SemiMA1_list = df2['pl_orbsmax'].tolist()
PMb_list = df2['pl_bmasse'].tolist()
PEb_list = df2['pl_orbeccen'].tolist()
POb_list = df2['pl_orbper'].tolist()
```

```
omega_b = df2['pl_orblper'].tolist()
EoP_b_list = df2['pl_orbtper'].tolist()
st_mass_list = df2['st_mass'].tolist()
st_teff = df2['st_teff'].astype(float)
st_teff_list = st_teff.tolist()
st_rad_list = df2['st_rad'].tolist()
st_lum_list = df2['st_lum'].tolist()

df3=df1.drop_duplicates(subset=['hostname'], keep='last') # keep second
    ↪ duplicate entry
PNc = df3['pl_name'].values.tolist()
PRc_list = df3['pl_rade'].values.tolist()
SemiMA2_list = df3['pl_orbsmax'].values.tolist()
PMc_list = df3['pl_bmasse'].values.tolist()
PEc_list = df3['pl_orbeccen'].tolist()
POc_list = df3['pl_orbper'].tolist()
omega_c = df3['pl_orblper'].tolist()
EoP_c_list = df3['pl_orbtper'].tolist()

#print(df.pl_tranmid)
#print(df.pl_orbtper)
#%%
def g(x): # convert planetary radii to mass
    return x**(1/0.59)

for n, i in enumerate(PMb_list): # replace 0 with estimate mass from their
    ↪  respective radii
    if i == 0.0:
        PMb_list[n] = g(PRb_list[n])

for n, i in enumerate(PMc_list): # replace 0 with estimate mass from their
    ↪  respective radii
    if i == 0.0:
```

```
       PMc_list[n] = g(PRc_list[n])

planetary_mass_b = [] # planetary mass in kg
planetary_mass_c = [] # planetray mass in kg
planetary_radii_b = [] # planetary radii in meters
planetary_radii_c = [] # planetary radii in meters
stellar_mass = [] # stellar mass in kg
planetary_mass_b_sol = [] #planetary mass in solar mass units
planetary_mass_c_sol = [] #planetary mass in solar mass units
planetary_orbit_b_years = [] #planetary orbit in years
planetary_orbit_c_years = [] #planetary orbit in years
host_star = HN1.tolist()
omega_b_rad = [] # omega in radians
omega_c_rad = [] # omega in radians
R_H=[]
K=[]
EoP_b_years = []
EoP_c_years = []
def h(x): # convert Earth-mass to kg
    return x * 5.97e24

def d(x): # convert Earth-radii to m
    return x * 6.378e6

def e(x): # convert Solar-mass to kg
    return x * 1.988e30

def l(x): # convert planetary mass from kg to solar units
    return x/1.988e30

def l1(x): # convert planetary orbit from days to years
    return x/365
```

```
def f(a_1,a_2,m_1,m_2,M_star): # calculate mutual hill radii (R_H)
    return ((a_1 + a_2)/2)*((m_1+m_2)/(3*M_star))**(1/3)

def k(a_1,a_2,r): # calculate K-value
    return (a_1-a_2)/r

def k1(x):
    return x * (np.pi/180)

for n in range(len(PMb_list)):
    planetary_mass_b.append(h(PMb_list[n]))
    planetary_mass_c.append(h(PMc_list[n]))
    planetary_radii_b.append(d(PRb_list[n]))
    planetary_radii_c.append(d(PRc_list[n]))
    stellar_mass.append(e(st_mass_list[n]))
    planetary_mass_b_sol.append(l(planetary_mass_b[n]))
    planetary_mass_c_sol.append(l(planetary_mass_c[n]))
    planetary_orbit_b_years.append(l1(POb_list[n]))
    planetary_orbit_c_years.append(l1(POc_list[n]))
    R_H.append(f(SemiMA1_list[n],SemiMA2_list[n],planetary_mass_b[n],
        ↪ planetary_mass_c[n],stellar_mass[n]))
    K.append(k(SemiMA2_list[n],SemiMA1_list[n],R_H[n]))
    omega_b_rad.append(k1(omega_b[n]))
    omega_c_rad.append(k1(omega_c[n]))
    EoP_b_years.append(l1(EoP_b_list[n]))
    EoP_c_years.append(l1(EoP_c_list[n]))

pl_orb_per_b_10 = [planetary_orbit_b_years[n]*0.1 for n in range(len(
    ↪ planetary_orbit_b_years))]
pl_orb_per_c_10 = [planetary_orbit_c_years[n]*0.1 for n in range(len(
    ↪ planetary_orbit_c_years))]
#print(pl_orb_per_c_10)
#print(planetary_orbit_b_years)
```

```
zippedList1 = list(zip(host_star, PNb, planetary_mass_b_sol, SemiMA1_list,
    ↪  omega_b_rad, PEb_list, planetary_orbit_b_years, pl_orb_per_b_10,
    ↪ EoP_b_years, PNc, planetary_mass_c_sol, SemiMA2_list, omega_c_rad,
    ↪ PEc_list, planetary_orbit_c_years, EoP_c_years, R_H, K, st_mass_list
    ↪ , st_teff_list, st_rad_list, st_lum_list))
dfx = pandas.DataFrame(zippedList1,columns=['host_name','planet b','
    ↪ pl_mass_b','semi_major_axis b', 'arg of periastron b [radians]', '
    ↪ eccentricity b', 'pl_orbper_b [years]', 'pl_orbper_b 10% [years]', '
    ↪ Epoch of Periastron b [years]', 'planet c','pl_mass_c','
    ↪ semi_major_axis c', 'arg of periastron c [radians]', 'eccentricity c
    ↪ ', 'pl_orbper_c [years]', 'Epoch of Periastron c [years]', 'R_H', 'K
    ↪ -values','stellar mass [M_sol]', 'effective temperature', 'stellar
    ↪ radii', 'stellar luminosity (solar)'])
dfx.drop(dfx.loc[dfx['K-values'] < 10].index, inplace=True)
dfx.sort_values(by='K-values', inplace=True, ascending=False)
#dfx.drop(dfx.loc[dfx['K_values'] > 100000].index, inplace=True)
dfx.drop(dfx.loc[dfx['effective temperature'] > 10000].index, inplace=True
    ↪ )
#dfx.drop(dfx.loc[dfx['stellar luminosity (solar)'] == 0.0].index, inplace
    ↪ =True)
stellar_temperature = dfx['effective temperature'].tolist()
stellar_luminosity = dfx['stellar luminosity (solar)'].tolist()
stellar_radii = dfx['stellar radii'].tolist()
sma_b = dfx['semi_major_axis b'].tolist()
sma_c = dfx['semi_major_axis c'].tolist()
dfx.reset_index(drop=True, inplace=True)
#print(dfx)

#%%
sigma = 5.670374419e-8 # [W/m^2T^4]
st_radii = [stellar_radii[i]*6.957e8 for i in range(len(stellar_radii))] #
    ↪  convert solar radii to meters
```

```
st_area = [4*np.pi*st_radii[i]**2 for i in range(len(st_radii))] # area in
    ↪  squared meters
st_temp = [stellar_temperature[i]/5777 for i in range(len(
    ↪ stellar_temperature))]

for n, i in enumerate(stellar_luminosity): # replace 0 with estimate
    ↪ luminosity from their respective radii and effective temperature
    if i == 0.0:
        stellar_luminosity[n] = np.log10(((stellar_radii[n]**2)*(st_temp[n
            ↪ ]**4)))
        #stellar_luminosity[n] = np.log10((sigma*st_area[n]*
            ↪ stellar_temperature[n]**4)/3.828e26)"""
#print(stellar_luminosity)
#%%
seff = [0,0,0,0,0,0]
seffsun = [1.776,1.107, 0.356, 0.320, 1.188, 0.99]
a = [2.136e-4, 1.332e-4, 6.171e-5, 5.547e-5, 1.433e-4, 1.209e-4]
b = [2.533e-8, 1.580e-8, 1.698e-9, 1.526e-9, 1.707e-8, 1.404e-8]
c = [-1.332e-11, -8.308e-12, -3.198e-12, -2.874e-12, -8.968e-12, -7.418e
    ↪ -12]
d = [-3.097e-15, -1.931e-15, -5.575e-16, -5.011e-16, -2.084e-15, -1.713e
    ↪ -15]



st_luminosity = [10**stellar_luminosity[i] for i in range(len(
    ↪ stellar_luminosity))]
starTemp = []
recentVenus = []
runawayGreenhouse = []
maxGreenhouse = []
earlyMars = []
fivemeRunaway = []
tenthmeRunaway = []
```

```
#print(st_luminosity)
for n in range(len(stellar_temperature)):
    tstar = stellar_temperature[n] - 5780.0
    for i in range(len(a)):
        seff[i] = seffsun[i] + a[i]*tstar + b[i]*tstar**2 + c[i]*tstar**3 +
            ↪ d[i]*tstar**4

    starTemp.append(stellar_temperature[n])
    recentVenus.append(seff[0])
    runawayGreenhouse.append(seff[1])
    maxGreenhouse.append(seff[2])
    earlyMars.append(seff[3])
    fivemeRunaway.append(seff[4])
    tenthmeRunaway.append(seff[5])



def d(x,y): # calculate HZ distance in AU
    return (x/y)**0.5

innerHZ_Venus = []
innerHZ_runaway = []
outerHZ_Mars = []
outerHZ_maxgreen = []
innerHZ_runaway_fiveme = []
innerHZ_runaway_tenthme = []

for i in range(len(starTemp)):
    innerHZ_Venus.append(d(st_luminosity[i],recentVenus[i]))
    innerHZ_runaway.append(d(st_luminosity[i],runawayGreenhouse[i]))
    outerHZ_Mars.append(d(st_luminosity[i],earlyMars[i]))
    outerHZ_maxgreen.append(d(st_luminosity[i],maxGreenhouse[i]))
    innerHZ_runaway_fiveme.append(d(st_luminosity[i],fivemeRunaway[i]))
```

```
    innerHZ_runaway_tenthme.append(d(st_luminosity[i],tenthmeRunaway[i]))



innerHZ_V = pandas.Series(innerHZ_Venus)
innerHZ_R = pandas.Series(innerHZ_runaway)
outerHZ_M = pandas.Series(outerHZ_Mars)
outerHZ_max = pandas.Series(outerHZ_maxgreen)
st_lum_new = pandas.Series(stellar_luminosity)
dfx.insert(16, 'Inner HZ - Venus', innerHZ_V)
#dfx.insert(3, 'Inner HZ - Runaway', innerHZ_R)
dfx.insert(17, 'Outer HZ - Mars', outerHZ_M)
#dfx.insert(6, 'Outer HZ - Max Greenhouse', outerHZ_max)
dfx.insert(21, 'Luminosity [L_sol]', stellar_luminosity)
dfx.drop(dfx.loc[dfx['semi_major_axis c'] <= dfx['Inner HZ - Venus']].
    ↪ index, inplace=True)
dfx.drop(dfx.loc[dfx['semi_major_axis b'] >= dfx['Outer HZ - Mars']].index
    ↪ , inplace=True)
dfx.drop('stellar luminosity (solar)', axis=1, inplace=True)
sma_b = dfx['semi_major_axis b'].tolist()
sma_c = dfx['semi_major_axis c'].tolist()
K_values = dfx['K-values'].tolist()
innerHZ_venus_new = dfx['Inner HZ - Venus'].tolist()
outerHZ_Mars_new = dfx['Outer HZ - Mars'].tolist()
dfx.reset_index(drop=True, inplace=True)
planetary_mass_b_new = dfx['pl_mass_b'].tolist()
planetary_mass_c_new = dfx['pl_mass_c'].tolist()
stellar_mass_new = dfx['stellar mass [M_sol]'].tolist()
print(dfx)

#%%
plt.figure(1)
plt.scatter(st_luminosity,innerHZ_Venus)
plt.xscale('log')
```

```
plt.yscale('log')
plt.xlabel('$\log_{10}(L)$ $[L_\odot]$')
plt.ylabel('Inner HZ Boundary - Venus [AU]')
plt.savefig("innerHZ.pdf")

plt.figure(3)
plt.scatter(st_luminosity,outerHZ_Mars)
plt.xscale('log')
plt.yscale('log')
plt.xlabel('$\log_{10}(L)$ $[L_\odot]$')
plt.ylabel('Outer HZ Boundary - Mars [AU]')
plt.savefig("outerHZ.pdf")

plt.figure(2)
plt.scatter(stellar_temperature,stellar_luminosity)
plt.xlabel('$T_{\mathrm{eff}}$ [K]')
plt.ylabel('$\log_{10}(L)$ $[L_\odot]$')
plt.gca().invert_xaxis()
plt.savefig("fig2.pdf")

#%%
plt.figure(6)
ax = dfx.plot.scatter(x='semi_major_axis b', y='host_name', label='Planets
    ↪ ', figsize=(6,7))
dfx.plot.scatter(x='semi_major_axis c', y='host_name', ax=ax)
dfx.plot.scatter(x='Inner HZ - Venus',marker='|', color='DarkGreen', y='
    ↪ host_name', label='HZ inner boundary', ax=ax)
dfx.plot.scatter(x='Outer HZ - Mars',marker='|', color='LightGreen', y='
    ↪ host_name', label='HZ outer boundary', ax=ax)
plt.xscale('log')
#plt.patches.rectangle()
plt.xlabel('$\log_{10}(\mathrm{Semi-major \; axis})$ [AU]')
plt.ylabel('Host Stars')
```

```
plt.gca().invert_yaxis()
plt.savefig("fig6.pdf", bbox_inches = "tight")
```

A.2 Running Simulations and Creating MEGNO Maps

```
from pylab import *
import numpy as np
from mpl_toolkits.mplot3d import axes3d
import pandas

def simulation(par):
    a, e = par # unpack parameters
    sim = rebound.Simulation()
    sim.units = ('yr', 'AU', 'Msun')
    sim.integrator = "whfast"
    sim.ri_whfast.safe_mode = 0
    sim.dt = 0.00059
    sim.add(m=0.94) # Star
    sim.add(m=0.001794, omega=0.296706, e=0.0110, P=0.005880, T
       ↪ =6730.626849)
    sim.add(m=0.007435, omega=1.937315, e=0.7100, P=13.287671, T
       ↪ =6730.783562)
    sim.add(a=a,e=e,omega=0,m=0.000003)
    #sim.add(m=0.000070, a=0.05254, omega=0.331613, e=0.2180)
    #sim.add(m=0.001523, a=4.1300, omega=2.508038, e=0.6010)
    #sim.add(m=0.000003, a=a, omega=0, e=e)
    sim.move_to_com()

    sim.init_megno()
    sim.exit_max_distance = 20.
    try:
```

```
        sim.integrate(5e2*2.*np.pi, exact_finish_time=0) # integrate for
            ↪ 500 years, integrating to the nearest
        #timestep for each output to keep the timestep constant and
            ↪ preserve WHFast's symplectic nature
        megno = sim.calculate_megno()
        return megno
    except rebound.Escape:
        return 10. # At least one particle got ejected, returning large
            ↪ MEGNO.

#print(simulation((7,0.1)))

Ngrid = 80
par_a = np.linspace(0.538878,1.288364,Ngrid)
par_e = np.linspace(0.,0.5,Ngrid)
parameters = []
for e in par_e:
    for a in par_a:
        parameters.append((a,e))
from rebound.interruptible_pool import InterruptiblePool
pool = InterruptiblePool()
results = pool.map(simulation,parameters)

results2d = np.array(results).reshape(Ngrid,Ngrid)
#%matplotlib inline
fig = plt.figure(figsize=(7,5))
ax = plt.subplot(111)
extent = [min(par_a),max(par_a),min(par_e),max(par_e)]
ax.set_xlim(extent[0],extent[1])
ax.set_xlabel("semi-major axis $a$")
ax.set_ylim(extent[2],extent[3])
ax.set_ylabel("eccentricity $e$")
```

```
im = ax.imshow(results2d, interpolation="none", vmin=1.9, vmax=4, cmap="
    ↪ RdYlGn_r", origin="lower", aspect='auto', extent=extent)
cb = plt.colorbar(im, ax=ax)
cb.set_label("MEGNO $\\langle Y \\rangle$")
plt.title("Pr0211 MEGNO Stability Map")
plt.savefig("Pr0211 - timestep=0.00059 - int=500.pdf")



#\%\%
semi_major_axis = [x[0] for x in parameters]
eccentricity = [x[1] for x in parameters]
zippedlist = list(zip(semi_major_axis, eccentricity, results))
df = pd.DataFrame(zippedlist,columns=['semi_major_axis', 'eccentricity', '
    ↪ MEGNO value'])
df.to_csv("Pr0211 - timestep=0.00059 - int=500.csv", index=False)
```

A.3 Calculating period ratios for HD 37605

```
G=6.67430e-11 #SI units
M=1.87e30 # stellar mass in kg
P_b=0.150720 # orbital period of planet b in years
#P_c=7.452055 # orbital period of planet c in years
a_AU=[0.6,0.73,0.84,0.95,1.05,1.15,1.25,1.34] #semi major axes of 1 Earth
    ↪ mass planet in AU
a_meters=[a_AU[n]*1.496e11 for n in range(len(a_AU))] #semi major axes of
    ↪ 1 Earth mass planet in meters

def period(a): #function defining orbital period
    T = 2*np.pi*((a**3)/(G*M))**0.5
    return T
P_earth=[period(a_meters[n])/(3.154e7) for n in range(len(a_meters))] #
    ↪ orbital period in years
```

```
P_ratio=[P_earth[n]/P_b for n in range(len(P_earth))] #P_out/P_in


print(P_ratio)
```

A.4 Assessing the possible co-orbital configuration of HIP 67851 and Teegarden's Star

```
import numpy as np
import matplotlib.pyplot as plt
import rebound

def simulation(par):
    a, e = par # unpack parameters
    sim = rebound.Simulation()
    sim.units = ('yr', 'AU', 'Msun')
    sim.integrator = "whfast"
    sim.ri_whfast.safe_mode = 0
    sim.dt = 0.001
    sim.add(m=0.09) # Star
    sim.add(m=0.000003, omega=1.343904, e=0.0000, P=0.013452, T
       ↪ =6734.389863)
    sim.add(m=0.000003, omega=4.991642, e=0.0000, P=0.031258, T
       ↪ =6734.392329)
    sim.add(a=a,e=e,m=0.000003)
    sim.move_to_com()
    ps = sim.particles

    sim.exit_max_distance = 20.

    Noutputs = 500
    year = 2.*np.pi # One year in units where G=1
    times = np.linspace(0., 500.*year, Noutputs)
```

```
    l1 = np.zeros((1, Noutputs))
    l2 = np.zeros((1, Noutputs))

    for i, time in enumerate(times):
        sim.integrate(time)
        l1[0][i] = ps[2].l # This stores the data which allows us to plot
            ↪ it later
        l2[0][i] = ps[3].l

    return np.subtract(l1, l2), times

angles_2pi = np.mod(angles, 2*np.pi)
delta_l, times = simulation((0.0443,0.03))
fig = plt.figure()
plt.scatter(times,delta_l)
ax = plt.subplot(111)
ax.set_xlabel("Time [$yrs$]")
ax.set_ylabel("Mean Longitude $\Delta$l [rad]")
plt.title("Teegarden's Star Co-orbital Configuration")
plt.savefig("Teegarden's Star - a=0.0443, e=0.03.pdf")
plt.show()
```

Appendix B

Figures

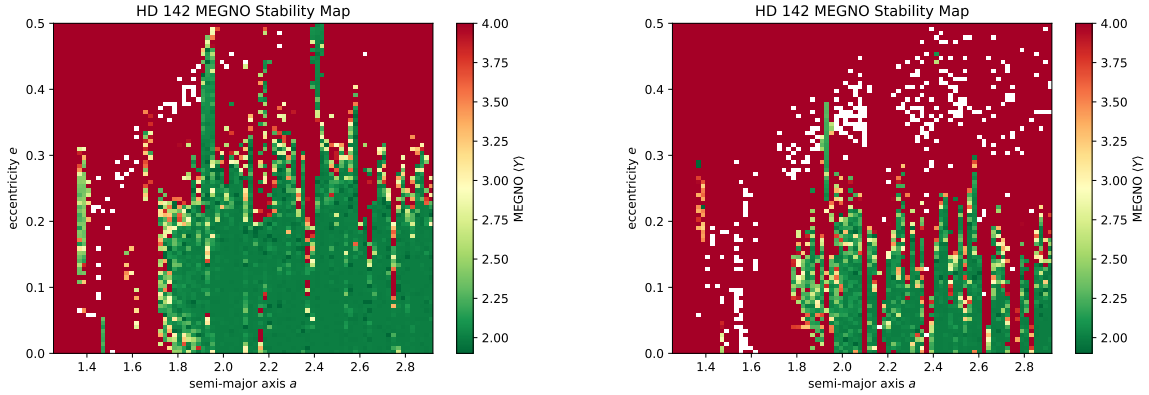

Figure B.1: HD 142 MEGNO stability map integrated over 500 years on the left panel and 5000 years on the right. Inserted planet's parameters: time-step = 0.0096 years, M = 0, $\omega = 0$.

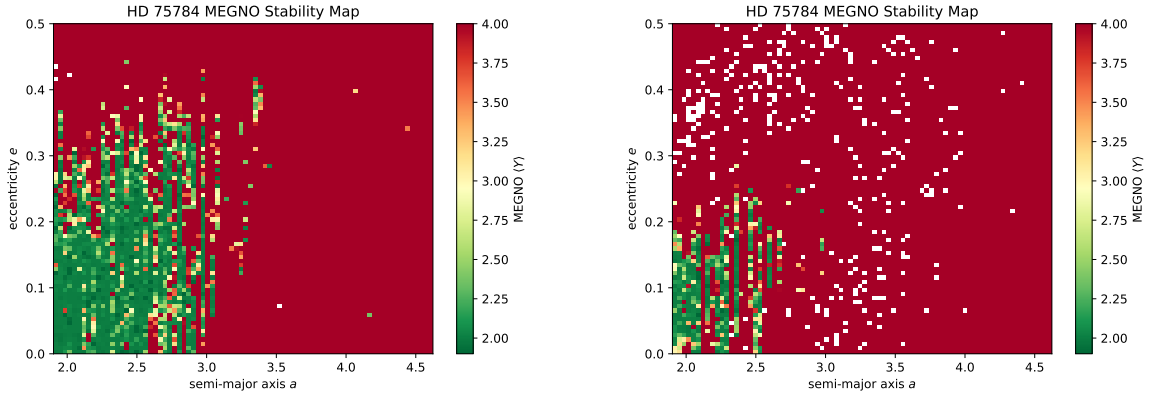

Figure B.2: HD 75784 MEGNO stability map integrated over 500 years on the left panel and 5000 years on the right. Inserted planet's parameters: time-step = 0.093 years, M = 0, $\omega = 0$.

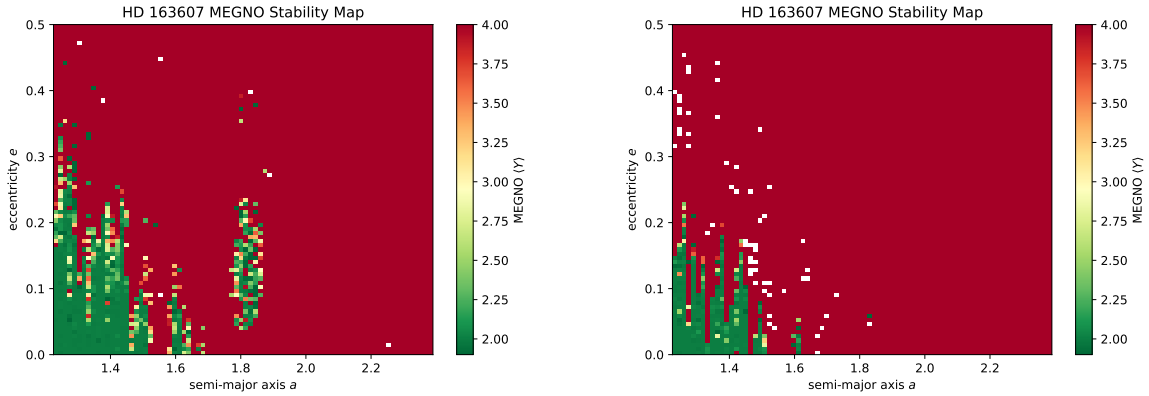

Figure B.3: HD 163607 MEGNO stability map integrated over 500 years on the left panel and 5000 years on the right. Inserted planet's parameters: time-step = 0.02 years, M = 0, $\omega = 0$.

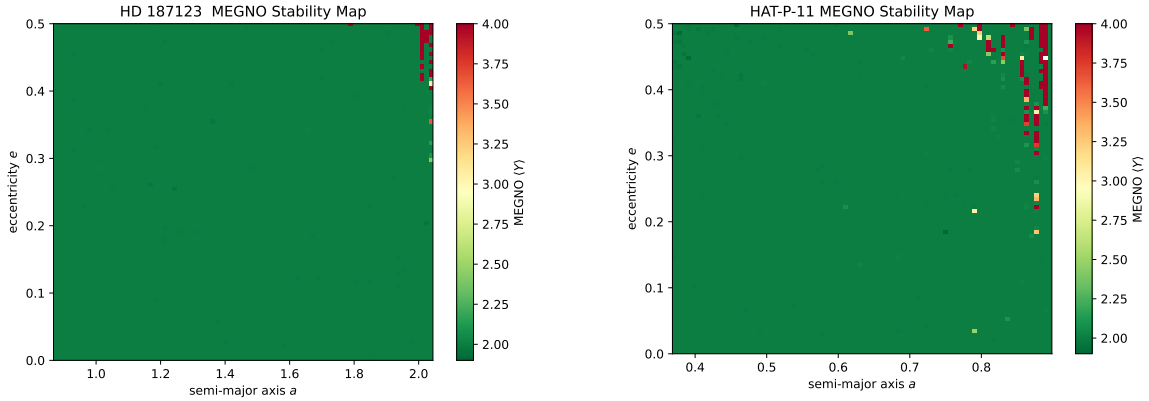

Figure B.4: Left: HD 187123 MEGNO stability map integrated over 500 years Inserted planet's parameters: time-step = 0.0008 years, M = 0, $\omega = 0$. Right: HAT-P-11 MEGNO stability map integrated over 500 years. Inserted planet's parameters: time-step = 0.001 years, M = 0, $\omega = 0$.

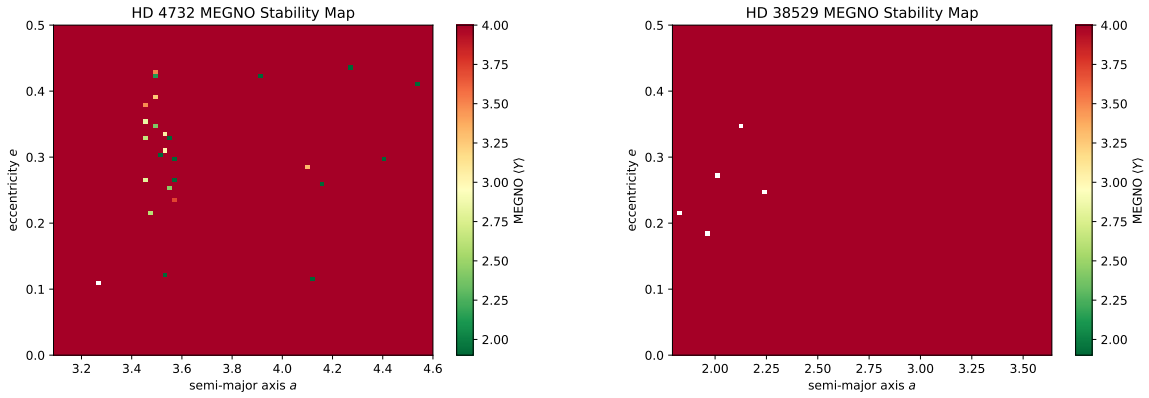

Figure B.5: Left: HD 4732 MEGNO stability map integrated over 500 years. Inserted planet's parameters: time-step = 0.099 years, M = 0, $\omega = 0$. Right: HD 38529 MEGNO stability map integrated over 500 years. Inserted planet's parameters: time-step = 0.004 years, M = 0, $\omega = 0$.

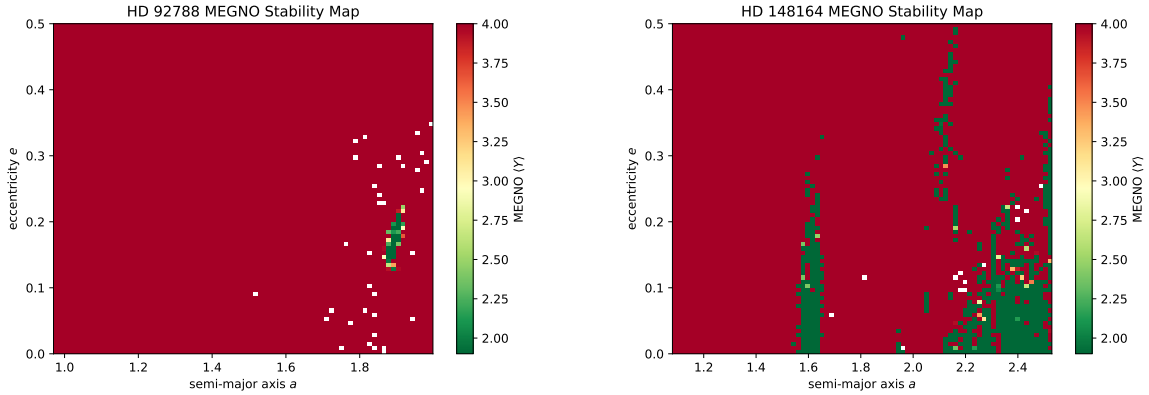

Figure B.6: Left: HD 92788 MEGNO stability map integrated over 500 years. Inserted planet's parameters: time-step = 0.089 years, M = 0, $\omega = 0$. Right: HD 148164 MEGNO stability map integrated over 500 years. Inserted planet's parameters: time-step = 0.09 years, M = 0, $\omega = 0$.